京都大学防災研究所年報 第 60 号 B 平成 29 年
DPRI Annuals, No. 60 B, 2017

A New Method of Stress Analysis in Hillslopes Considering Vegetation Effects Using Poroelasticity

Ying-Hsin WU and Eiichi NAKAKITA

Synopsis

This study presents a new methodology of stress analysis for a steep and vegetated hillslope. A hillslope is modelled as a poroelastic medium under influences of vegetation surcharge on the surface and root-reinforcement inside. Tree-growth allometric equations are used for quantitative modelling of transient tree surcharge and root-reinforcement. Poroelasticity is used for evaluating stress equilibrium inside the slope of any geometry under given conditions of groundwater flow and vegetation forcing. Then, Mohr-Coulomb failure theory is applied to find the unstable zones. The three parts above are numerically solved by using the finite element method. We performed case study of saturated hillslopes in different two-dimensional geometries. The results testified this method can assess the stability of vegetated hillslope in any two-dimensional geometry.

Keywords: vegetation, poroelasticity, Mohr-Coulomb theory, finite element analysis, stress field, slope stability

1. Introduction

In recent decades, people around the world have experienced that hot days happened more frequently, temperature became a bit higher, and rainfall occurred shorter in time but more severe in intensity. These rare phenomena of extreme climate have caused many areas worldwide suffering from more natural disasters than the past. Under this global warming tendency, it is unavoidable that these extreme climate phenomena will become the usual situation to cause more disasters. In the global view, mountainous area recently becomes more vulnerable for landslide disasters due to more frequent extreme rainfall (Kirschbaum et al., 2012), and a tendency of increasing landslide and debris flow disasters has been revealed (Gariano and Guzzetti, 2016). In the localized view, extreme rainfall can trigger massive shallow landslides, e.g., debris flow disasters in Hiroshima in 2014 (Wang et al., 2014), or deep-seated landslides, e.g., in Nara during Typhoon Talas in 2011 (Chigira et al., 2013; Chigira, 2014), on hillslopes where used to be safe and stable. To pursue a safer slopeland in the future, an analysis of hillslope safety under climate change influence is certainly important and necessary. In this study, we would like to propose a methodology applicable to evaluate the

hillslope safety considering climate change effects.

From the mechanical perspective, hillslope stability depends on stress equilibrium of soil resistance against driving forces, e.g. groundwater motion, internal strength and external loading on slopes. Processes influencing stress status in a hillslope can be revealed from hydrological, geotechnical, geological, biological, or other factors (Sidle and Bogaard, 2016). As trying to investigate the long-term interaction between climate and hillslope safety, we consider the vegetation impacts, and focus on the analysis of vegetated hillslopes under the hydrometeo-rological influences of groundwater flows altered by extreme rainfall as well as the bioenvironmental effects of vegetation weight and root reinforcement.

In last decades, a great amount of landslide models have been proposed based on several different methods, e.g., statistical models (e.g., Ono et al., 2011; Budimir et al., 2015), one-dimensional infinite slope stability models (e.g., Montgomery and Dietrich, 1994; Baum et al., 2010), multi-dimensional slope stability models (e.g., Milledge et al., 2014; Bellugi et al., 2015); and poroelasticity (e.g., Iverson and Reid, 1992; Goren and Aharonov, 2009). Each model has been successfully verified by some historical events or laboratory experiments. Statistical models are robust and easy to be formulated for any area with sufficient event samples, but may not be able to estimate the long-term dynamical interaction. More complicated than statistical models, mechanical ones are good at physically representing hillslope processes. However, most of present mechanical models are usually derived in terms of the infinite slope stability model with simplified assumption of groundwater flow parallel to the bedrock. Because the infinite slope stability model adopts the plastic theory (Terzaghi, 1948), an accurate calculation of plasticity requires information of failure surface which is unknown in priori for a natural hillslope. Therefore, utilizing poroelasticity for direct analysis of stress field can overcome the drawback of lacking of failure surface information. Hence, in the last decades poroelasticity has been widely applied to analysis of an engineering slope of infinite depth (e.g., Terzaghi, 1948; Iverson and Reid, 1992; Das 2014). But, it comes out another problem that the depth of soil layer above bottom bedrock in hillslope is usually finite. Therefore, correct assessment of stress field by using poroelasticity argues information of soil layer depth and one additional no displace-ment boundary condition at soil-layer bottom. To better assess hillslope safety in the future, we adopt the method of poroelasticity.

The other important factor influencing the slope stability is vegetation. The vegetation on hillslope can stabilize the slope by its weight on the surface, and can enhance soil strength by root-reinforcement. Recently, based on the forest allometry, the aboveground mass (AGB) and belowground mass (BGB), representing the vegetation weight above and under the slope surface, in different climatological zones can be quantitatively estimated (Chave et al., 2005). Besides, vegetation can also be altered by climate conditions. Therefore, we take vegetation surcharge and additional root-reinforcement cohesion into account in our methodology as important biological factors for solving stress field in a slope.

In the following, the content starts by brief introduction of all fundamental theories and numerical methods we adopted. Then, it follows the case analysis, result and discussion, and concluding remarks.

2. Problem setup and fundamental theory

In most cases, depth of natural hillslopes can be regarded to be finite. To analyze finite-depth hillslopes, our methodology comprises four parts: a) estimation of vegetation surcharge and root reinforcement, b) groundwater motion, c) effective stress field analysis,

and d) soil failure analysis. Each part shall be briefly introduced in the following. In this study, we consider the two-dimensional problems.

2.1 Soil thickness estimation

The soil depth of a natural hillslope is usually finite. Because the exact soil thickness is usually unavailable without field investigation, some geomorphological relations (Catani et al., 2010), depending on the local slope angle or other parameters, can be used for approximate thickness estimation within a reasonable error.

2.2 Vegetation effects on a hillslope

Being an important factor for carbon cycle analysis, aboveground biomass (AGB) and belowground biomass (BGB) have been widely used for estimating vegetation weight based on tree allometry (Chave et al., 2005). With AGB from allometric equations the vegetation loading W can be estimated by

$$W = \mathrm{AGB} \times A \,, \tag{1}$$

where A is the area. To express the effect of root-reinforcement on a soil bulk (Wu, 2013), the total cohesion of soil bulk can be expressed as

$$c = c_s + c_r \,, \tag{2}$$

where c_s is the original soil cohesion [Pa], and c_r stands for the additional cohesion [Pa] due to root-reinforcement. In most tree species, c_r has an exponentially decaying profile in the perpendicular direction of the soil layer, but has different horizontal extents (Dupuy et al. 2010).

2.3 Evaluation of stress field in the soil layer

A hillslope can be modelled as a poroelastic medium (Biot 1941; Iverson and Reid, 1992), which regards soil bulk as an elastic skeleton and water or air fills up the interior voids. To connect groundwater effect with an elastic soil bulk, it is conventional to adopt the common effective stress σ'_{ij} (Terzaghi, 1948), as below

$$\sigma'_{ij} = \sigma_{ij} + p\delta_{ij} \,, \tag{3}$$

where p is the pore water pressure [Pa], σ_{ij} is the stress tensor and δ_{ij} is the Dirac delta function, where indices $(i,j) = \{x, z\}$ as the present work focus on two-dimensional problems in the Cartesian coordinates. Under the assumption of linear elastic medium and infinitesimal strain, (3) can be expressed by the relationship between stress and displacement,

$$\sigma'_{ij} = \lambda\left(\frac{\partial u_k}{\partial x_k} + p\right)\delta_{ij} + \mu\left(\frac{\partial u_i}{\partial u_j} + \frac{\partial u_j}{\partial u_i}\right), \tag{4}$$

where λ and μ are Lamé constants, and u_i denotes the displacement vector. The Lamé constants can also be expressed as

$$\lambda = \frac{E\nu}{(1+\nu)(1-2\nu)} \quad \text{and} \quad \mu = \frac{E}{2(1+\nu)} \tag{5}$$

where E is the Young's modulus, and ν is the Poisson ratio of a soil bulk. Also, with (3) the stress equilibrium of a finite-depth soil layer reads

$$\frac{\partial \sigma'_{ij}}{\partial x_j} = \frac{\partial p}{\partial x_i} - \rho f_i + \rho \frac{\partial u_i}{\partial t} \,, \tag{6}$$

where σ'_{ij} is the tensor of effective stresses [Pa], $f_i = (0, 0, -g)$ stands for the gravitational effect [Pa/m], ρ is the constant bulk density [kg/m^3] and g is the gravitational acceleration [m^2/s]. Then, for elastic soil, the effective stress compatibility gives

$$\frac{\partial^2 \sigma'_{ii}}{\partial x_j \partial x_j} = \frac{1}{1-\nu} \frac{\partial^2 p}{\partial x_j \partial x_j}, \quad (7)$$

where $\partial^2 / \partial x_j \partial x_j$ represents the Laplace operator.

Finally, it requires pore water pressure information for stress equilibrium. As being the conventional theory of groundwater flow, the Richards' equation (Brutsaert, 2005) is adopted in our study, as below

$$k_i \frac{\partial^2}{\partial x_j \partial x_j} \left(\frac{p}{\rho_w g} + x_i \delta_{zi} \right) = S_s \frac{\partial H}{\partial t} - R, \quad (8)$$

where k_i denotes the hydraulic conductivity [m/s] in the *i*-direction, S_s is the specific storage [m^{-1}], R is the rainfall recharge [s^{-1}] , and the hydraulic head H [m] is defined as

$$H = p / \rho_w g + x_i \delta_{zi},$$

and ρ_w is the water density [kg/m^3], and $\delta_{zi} = 1$ if $i = z$ otherwise $\delta_{zi} = 0$.

Boundary conditions are no deformation at the lateral and bottom boundaries, i.e.,

$$u_i = 0, \text{ at } z = 0, \ x = B_L \text{ and } B_R, \quad (9)$$

and tractions at the top surface of a slope as

$$\sigma'_{ij} n_j = W \delta_{zi} \text{ and } p = 0, \text{ at } z = h(x). \quad (10)$$

For a saturated condition, $p(z = h) = 0$ is imposed on the slope surface with fluxes at lateral interfaces and no bottom flux. Particularly, the surface influx, representing the infiltration motion of unsaturated soil, can also be assumed as boundary conditions for solving (8) separately.

As the geometry of a real hillslope is usually not a simple rectangle, the governing equations, from (3) to (10), are numerically solved by using the finite element method. Then, the method of stress analysis is verified by analytical solutions of problems in a simple geometry.

2.4 Soil failure analysis

The Mohr-Coulomb theory (Terzaghi, 1948) is used for identifying unstable zones. Considering vegetation influences, the root-reinforced cohesion (2) and solved stresses are applied to find the location of a possible failure surface. The yield function F of failure surface reads

$$F = (\sigma_{xx} - \sigma_{zz})^2 - \sin^2 \phi (\sigma_{xx} + \sigma_{zz} + 2c / \tan \phi)^2, \quad (11)$$

where σ_{xx} and σ_{zz} are the principal stresses, ϕ is the friction angle [°] of soil bulk, $F < 0$ denotes no failure, and $F = 0$ can give the failure surface.

3. Numerical method

As the governing equations, from (3) to (10), are linear, the conventional finite element method (Zienkiewicz et al., 2013) is used for numerically evaluating approximate stress field in a hillslope. For finite element analysis, the weak (or variational) formulation of stress equilibrium reads

$$\int_\Omega \frac{\partial (\delta u_i)}{\partial x_j} \sigma'_{ji} d\Omega = \int_{\Gamma_h} (\delta u_z) W d\Gamma + \int_\Omega (\delta u_i) \left[\beta \left(\frac{\partial h}{\partial x_i} - \delta_{zi} \right) - g \delta_{zi} \right] d\Omega, \quad (12)$$

where δu_i is a vectorial test function of displacement; Ω and Γ_h denote the whole domain and boundary of slope surface, respectively.

The weak formulation of groundwater motion is

$$\int_{\Omega} k \frac{\partial(\delta h)}{\partial x_j} \frac{\partial h}{\partial x_j} d\Omega = \int_{\Gamma_q} (\delta h) \bar{q} d\Gamma + \int_{\Omega} (\delta h) \left(C \frac{\partial h}{\partial t} - Q \right) d\Omega, \quad (13)$$

where δh is a scalar test variable of hydraulic head; Γ_q denotes the lateral interfaces for in or out-flux.

Equations (12) and (13) also stand for the variational formulation of the governing equations in the three dimensions. To solve the above variational formulations of our problem, the numerical program was implemented with the help of a free and well-developed finite element solver, which is called freefem++ (Hecht, 2012).

4. Analysis and discussion

Two-dimensional slopes in different geometries are used for analysis and verification of applicability of our proposed methodology.

4.1 Problem setup

We consider the hillslopes covered by a natural forest of which the main tree species is *Japanese Cedar*. For a hillslope, the vegetation surcharge on the surface and root-reinforcement underground can estimated using allometric equations. Initial condition is set to be no vegetation in the beginning, as is shown in Fig. 1 (derivation details are mentioned in the Appendix). As the tree growth is a long-term process, the time interval is set to be year, and total duration is 200 years. So, the transient effect in the stress equilibrium and groundwater flow equations, i.e., (6) and (8) respectively, can be ignored. This means the governing equations become steady-state ones, and the rainfall recharge R can be neglected in the time-scale of year. For such a long characteristic time, the infiltration process is also excluded, and only the full saturation is considered in this study. Then, four slope

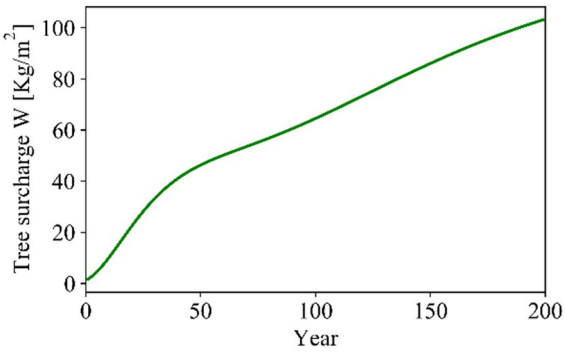

Fig. 1 Time variation of tree surcharge W

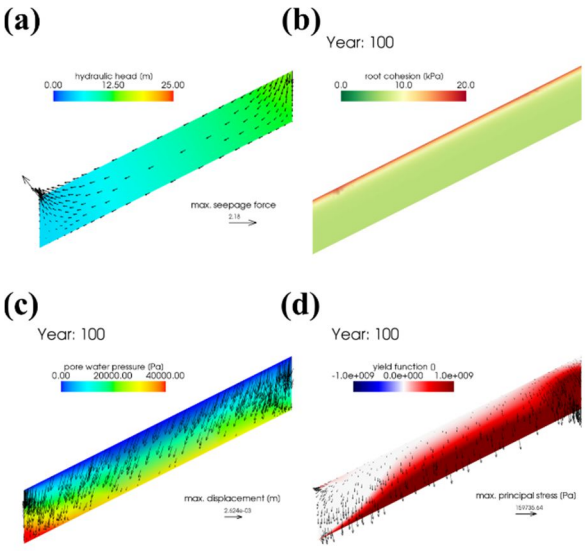

Fig. 2 Results of a saturated parallel slope. (a) pore-water pressure and seepage flow, (b) cohesion distribution due to root-reinforcement, (c) effective stress and displacement, and (d) yield function. The (b), (c), and (d) represents the results at the 100th year in our simulation.

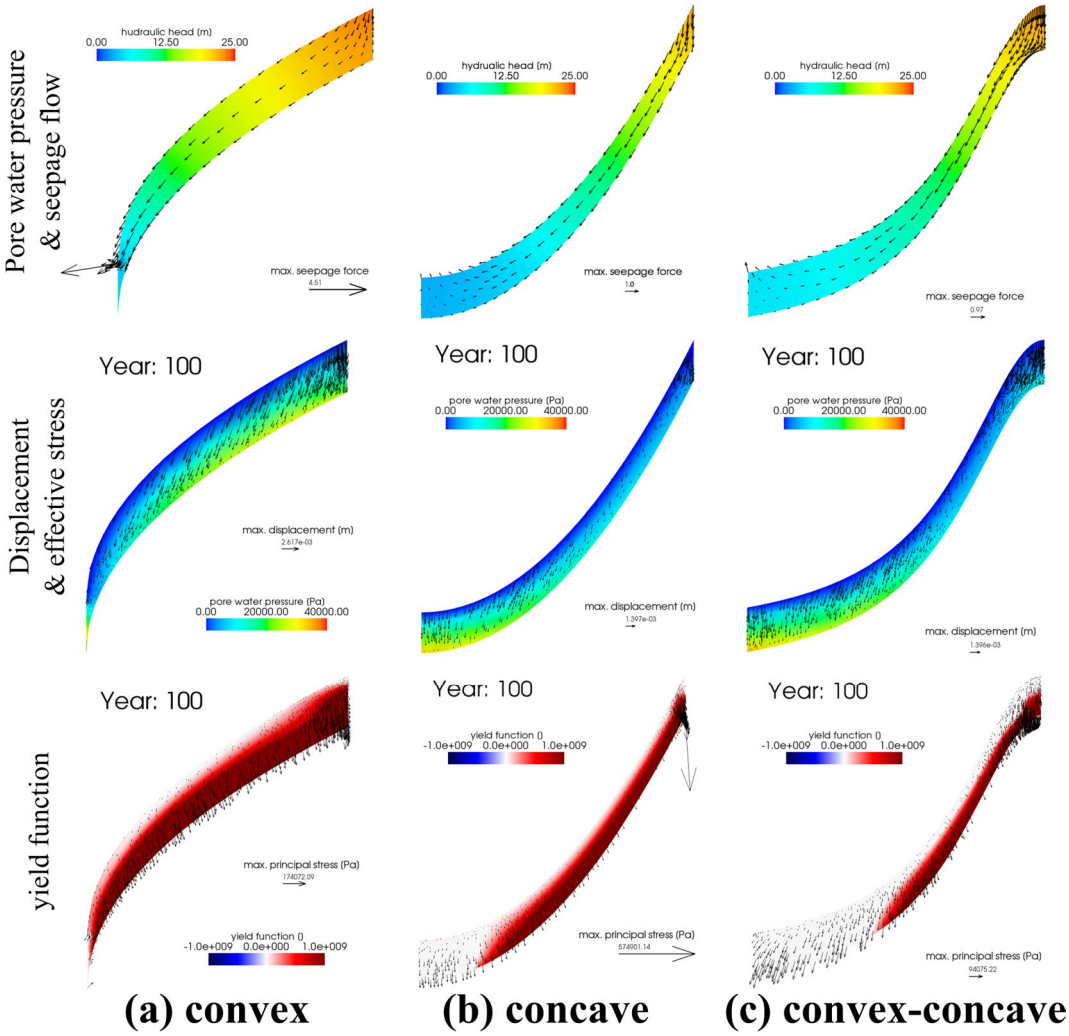

Fig. 3 Results of slopes in the geometries of (a) convex, (b) concave, and (c) convex-concave slopes. The data for demonstration is at 100 years. From up to down, subfigures show the pore-water pressure, slope displacement, and yield function for searching unstable zones.

shapes are used for analysis, including parallel, convex, concave, and convex-concave shapes, as are shown in Figs. 2 and 3.

Finally, we consider the general slopes consisting of loose sand and gravel, and referred to Das (2014) the soil parameters of the hillslopes are assumed to be Poisson ratio $\nu = 0.25$, Young's modulus $E = 80$ [MPa], soil density $\rho = 1,990$ [kg/m^3], soil cohesion $c = 7$ [kPa], and soil internal friction angle $\phi = 35^\circ$. For groundwater flow analysis, all the parameters are water density is $\rho_w = 1,000$ [kg/m^3] and hydraulic conductivity of homogeneous soil in slope is $k = 10^{-5}$ [m/s]. As the slope saturated, we here consider that no flux exists at the lateral boundary interfaces.

4.2 Results ad discussion

The analysis results of the fully-saturated slopes in the four different geometries are discussed in the following. The transient effect of tree surcharge is not significant in our cases as the tree weight is not heavier than the soil one. Figure 2 shows the results of parallel slopes. As saturation is assumed, the seepage flow is along in the slope boundaries, but not parallel everywhere, as in Fig. 2a. According to the vertical

tree root distribution adopted in this study, (19), the additional root-reinforcement cohesion concentrates in the portion near slope surface. Then, we can easily discover that effective stress directs to the slope downside, and the failure surface of unstable zone is not parallel to the top and bottom surfaces, as are shown in Fig. 2c and 2d. These reflect that the conventional assumption of parallel failure is invalid.

In the other three cases, Figure 3 shows the results of convex, concave, and convex-concave slopes. From stress distributions, higher effective stress exists in the downside of the concave-based slopes, but it can be found in the upside of the convex slope, as are shown in Fig. 3. This stress distributions reveal that the surface part is likely to be more unstable in a convex slope than in a concave one. The concave slopes have more resistance support from the downside of slope. Also, the failure surface is not parallel to the top and bottom boundaries. This result explains that a model without parallel failure assumption is more applicable to correctly analyze the safety of a hillslope of a finite depth.

5. Concluding remarks

We applied the poroelasticity with forest allometric models to analyze stress field in a vegetated hillslope, and conducted several case studies of two-dimensional slopes in different geometry and of a finite depth. From the results of case study, we found that the slope stability only changes a little bit as time evolves, and the convex slope has more unstable zone in the upside than concave and convex-concave slopes. The toe of a concave slope is an important part for resisting the slope from sliding failure.

For the next research steps in the future, theories and numerical methods of transient groundwater motion will be involved into this methodology to evaluate the time-dependent slope instability in a time interval shorter than a year. Then, the methodology will be available for analysis of slope safety under the effects of short-term extreme rainfall. Also, the model will be extended to a three-dimensional one. Some of real events will be conducted for verification. Finally, this methodology is expected to be a proxy to connect the analysis of hillslope stability with the climate change influence, and to be a new tool for risk assessment of slopeland area under future climate change.

Acknowledgement

The authors would like to thank the financial support from Japan Society for the Promotion of Science (JSPS) through the Grant-in-aid for JSPS Fellows (Grant No. 16F16378). YHW also deeply appreciates the support of JSPS Postdoctoral Fellowship for Overseas Researchers.

References

Baum, R.L., Godt, J.W., and Savage, W.Z. (2010): Estimating the timing and location of shallow rainfall-induced landslides using a model for transient, unsaturated infiltration, J. Geophys. Res. Earth Surf., Vol. 115, F03013.

Bellugi, D., Milledge, D.G., Dietrich, W.E., Perron, J.T., McKean, J. (2015): Predicting shallow landslide size and location across a natural landscape: Application of a spectral clustering search algorithm, J. Geophys. Res. Earth Surf., Vol. 120, pp. 2552-2585.

Biot, M.A. (1941): General theory of three - dimensional consolidation, J. Appl. Phys., Vol. 12, pp. 155-164.

Brutsaert, W. (2005): Hydrology: an introduction, 2nd edition, Cambridge University Press.

Budimir, M.E.A., Atkinson, P.M., and Lewis, H.G, (2015): A systematic review of landslide probability

mapping using logistic regression, Landslides, Vol. 12, No. 3, pp. 419-436.

Catani F., Segoni, S., and Falorni, G. (2010): An empirical geomorphology-based approach to the spatial prediction of soil thickness at catchment scale, Water Resour. Res., Vol. 46, W05508.

Chave, J., et al. (2005): Tree allometry and improved estimation of carbon stocks and balance in tropical forests, Oceologia, Vol. 145, pp. 87-99.

Cheng, C.H., et al. (2013): Biomass carbon accumulation in aging Japanese cedar plantations in Xitou, central Taiwan, Botanical Studies, Vol. 54, 60.

Chigira, M. (2014): Geological and geo - morphological features of deep-seated catastrophic landslides in tectonically active regions of Asia and implications for hazard mapping, Episodes, Vol. 37, No. 4, pp. 284-294.

Chigira, M., Tsou, C.Y., Matsushi, Y., and Matsuzawa, M. (2013): Topographic precursors and geological structures of deep-seated catastrophic landslides caused by Typhoon Talas, Geomorphology, Vol. 201, pp. 479-493.

Das, B.M. (2014): Advanced Soil Mechanics, Fourth Edition, CRC Press.

Dupuy L., Gregory P.J., and Bengough G. (2010): Root growth models: towards a new generation of continuous approaches, J. Exp. Bot., Vol. 61, No. 8, pp. 2131 -2143.

Gariano, S.L. and Guzzetti, F. (2016): Landslides in a changing climate, Earth-Sci. Rev., Vol. 162, pp. 227-252.

Genet, M., et al. (2008): Root reinforcement in plantations of *Cryptomeria japonica* D. Don: effect of tree age and stand structure on slope stability, Forest Ecol. Manag., Vol. 256, pp. 1517-1526.

Goren, L. and Aharonov, E. (2009): On the stability of landslides: A thermo-poro-elastic approach, Earth Planet. Sci. Lett., Vol. 277, pp. 365-372.

Hecht, F. (2012): New development in freefem++, J. Numer. Math., Vol. 20, No. 3-4, pp. 251–265.

Iverson, R.M. and Reid, M.E. (1992): Gravity-Driven Groundwater Flow and Slope Failure Potential 1. Elastic Effective-Stress Model, Water Resour. Res., Vol. 28, No. 3, pp. 925-938.

Kirschbaum D., Adler, R., Adler, D., Peters-Lidard, C., and Huffman, G. (2012): Global distribution of extreme precipitation and high-impact landslides in 2010 relative to previous year, J. Hydrometeorol., Vol. 13, pp. 1536-1551.

Milledge D.G., Bellugi, D., McKean, J.A., Densmore, A.L., and Dietrich, W.E. (2014): A multidimensional stability model for predicting shallow landslide size and shape across landscapes, J. Geophys. Res. Earth Surf., Vol. 119, pp. 2481-2504.

Montgomery, D.R. and Dietrich, W.E. (1994): A physically based model for the topographic control on shallow landsliding, Water Resour. Res., Vol. 30, No. 4, pp. 1153-1171.

Ono, K., Akimoto, T., Gunawardhana, L.N., Kazama, S., and Kawagoe, S. (2011): Distributed specific sediment yield estimates in Japan attributed to extreme-rainfall-induced slope failures under a changing climate, Hydrol. Earth Syst. Sci., Vol. 15, pp. 197-207.

Sidle, R.C. (1992): A Theoretical Model of the Effects of Timber Harvesting on Slope Stability, Water Resour. Res., Vol. 28, No. 7, pp. 1897-1910.

Sidle, R.C. and Bogaard, T.A. (2016): Dynamic earth system and ecological controls of rainfall-initiated landslides, Earth-Sci. Rev., Vol. 156, pp. 275-291.

Terzaghi, K. (1948): Theoretical Soil Mechanics, John Wiley and Son.

Wang, F., Wu, Y.H., Yang, H., Tanida, Y., and Kamei, A. (2015): Preliminary investigation of the 20 August 2014 debris flows triggered by a severe rainstorm in Hiroshima City, Japan, Geoenvironmental Disasters Vol. 2, No. 17.

Wu, T.H. (2013): Root reinforcement of soil: review of

analytical models, test results, and application of design, *Can. Geotech. J.*, Vol. 50, pp. 259-274.

Zienkiewicz, O.C., Taylor, R.L., and Zhu, J.Z. (2013): The Finite Element Method: Its Basis & Fundamentals, 7th edition, Elsevier.

Appendix

The derivation of growth equations of biomass weight, root strength, and root distribution of *Japanese Cedar* is presented here.

Firstly, the derivation of tree surcharge is mentioned as follows. Referring to the measurement (Cheng et al., 2013), the time evolution of the diameter at breast height (DBH), defined as the diameter of a tree trunk at 130 cm above ground, is expressed as

$$\mathrm{DBH} = 67\left(1 - 0.937\exp\left(-0.0117t\right)\right), \qquad (14)$$

where the unit of DBH is [cm], and t is the time in year, as shown in Fig. 4. Then, for the forests in Japan the allometric equation of aboveground biomass (Chave et al., 2015), representing the total weight of tree trunk, branches, and leaves, could be

$$\mathrm{AGB} = \rho_t \exp\left(-1.499 + 2.1481\Delta + 0.207\Delta^2 - 0.0281\Delta^3\right), \qquad (15)$$

where ρ_t is the averaged density [Mg/m^3] in the range of $0.302 \le \rho_t \le 0.442$ (Cheng et al., 2013), and $\Delta = \ln\left(\mathrm{DBH}\right)$. The next parameter is the distribution density N, of which the unit is the tree number in one square meter, can be expressed as

$$N = 0.036\left(1 + 10.112\exp\left(-0.0419t\right)\right). \qquad (16)$$

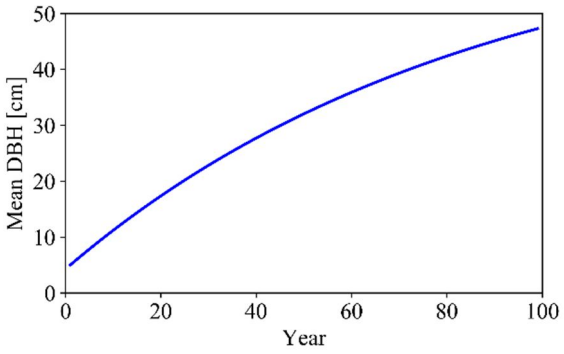

Fig. 4 Time variation of the mean diameter at breast height (DBH)

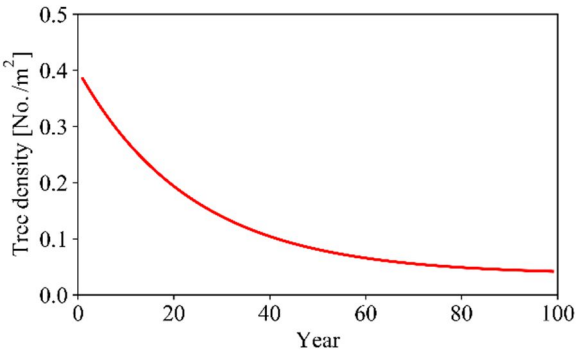

Fig. 5 Time variation of tree distribution density

Figure 5 shows the time variation of tree distribution density. The time-varying tree density in a unit area is an exponentially decay function because a tree can occupy more space as it grow up. Finally, using (14) to (16) the tree surcharge in a unit area [kg/m^2] yields

$$W\left(t\right) = N \times AGB, \qquad (17)$$

which is one boundary condition at the slope surface for stress equilibrium analysis. Figure 1 shows the time variation of tree surcharge.

On the other hand, the time evolution of additional cohesion in terms of growth of tree root in hillslope can also be quantitatively modelled by allometric equations. The time-dependent root cohesion (Sidle,

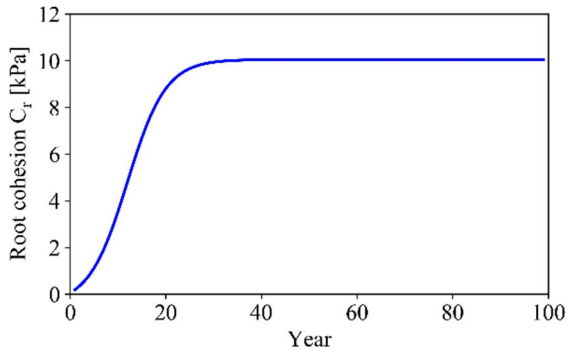

Fig. 6 Time variation of additional cohesion at the slope surface due to root-reinforcement

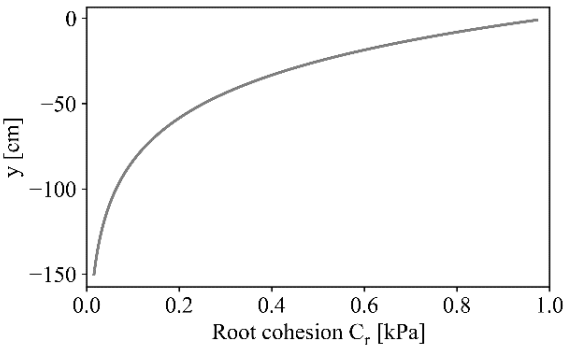

Fig. 7 Vertical profile of additional root cohesion

1992) can be expressed as

$$R(t) = \frac{10}{0.952 + 19.05\exp(-0.25t)} - 0.449\,, \tag{18}$$

where the unit of is [kPa]. From measured data (Genet et al., 2008) the vertical normalized distribution of root can be an exponential-decaying function, as below

$$D(z) = \exp(-0.0275z)\,. \tag{19}$$

Finally, combining (19) and (20) yields the spatiotemporal distribution of additional cohesion due to root-reinforcement within a hillslope as below,

$$c_r(z,t) = R \times D\,. \tag{20}$$

Figures 6 and 7 show the growth curve of additional root-reinforcement cohesion and the vertical root distribution, respectively.

Equation (17) is used as a boundary condition at the slope surface for evaluation of stress equilibrium, and (20) is applied to Mohr-Coulomb failure theory for identifying the unstable zones.

(Received June 13, 2017)